Available online at www.sciencedirect.com
ScienceDirect
Journal of Catalysis 247 (2007) 61–67
JOURNAL OF CATALYSIS
www.elsevier.com/locate/jcat

Lithium ion induced surface reactivity changes on MgO nanoparticles

Thomas Berger [a], Johannes Schuh [b], Martin Sterrer [a,1], Oliver Diwald [a,*], Erich Knözinger [a]

[a] *Institute of Materials Chemistry, Vienna University of Technology, Veterinärplatz 1/GA, A-1210 Vienna, Austria*
[b] *Institute of Chemical Technologies and Analytics, Vienna University of Technology, Getreidemarkt 9/164, A-1060 Vienna, Austria*

Received 21 June 2006; revised 24 October 2006; accepted 12 January 2007

Available online 14 February 2007

Abstract

Aiming at an estimate of the number of chemically active surface defects on MgO nanocrystals, we used Li^+ doping in conjunction with subsequent thermal annealing. Changes in the surface reactivity of the Li^+-doped nanocrystals were monitored by IR and electron paramagnetic resonance spectroscopy using chemisorbed hydrogen, surface trapped electrons, and surface complexed O_2^- as molecular probes. It was found that the admixture of 0.2 at% Li^+ not only significantly reduces the thermal stability, but also changes all surface spectroscopic features specific to pure MgO. On the basis of the Li^+ doping effect, the maximum concentration of active surface sites on undoped MgO nanocrystals corresponds to 3% of a nanocrystal monolayer.

Keywords: Lithium segregation; MgO nanostructures; Surface doping; Oxide nanostructures; Surface defect concentration; Grain coarsening; Spectroscopic surface probes

1. Introduction

Insights into electronic structure and chemical surface reactivity of polycrystalline materials are important for heterogeneous catalysis, engineering of nanomaterials, and the definition of new device concepts on the nanoscale. We have shown in previous work that MgO nanoparticles can be produced by chemical vapor deposition and that the choice of the production parameters sets the average size of the particles [1]. MgO nanoparticles appear to be outstanding building blocks for the construction of functional nanostructures and mesostructures and to serve as suitable model systems for the investigation of surface reactivity on oxides. Pure alkaline earth oxides (AEOs) have been intensively investigated in the fields of surface science and catalysis [2–11] due to their simple crystal structure and perfect ionicity. Furthermore, the MgO surface can be effectively doped with selected impurities by making use of thermally induced impurity segregation into the surface [12,13]. As demonstrated for mixed $Ca_xMg_{1-x}O$ particles, this can lead to unexpected optical and chemical surface properties [14,15].

The motivation for the present investigation has been to elucidate how traces of Li impurities affect the surface properties of the MgO nanoparticles. The close ionic radius of Li^+ ($r_{Li^+} = 0.76$ Å) compared with that of Mg^{2+} ($r_{Mg^{2+}} = 0.72$ Å) allows for easy substitutional accommodation within the MgO lattice. After thermal treatment, Li^+ ions tend to localize in the surface and near-surface region of the MgO-based crystallites [16]. They induce defects that are important for heterogeneous catalysis, where Li-promoted MgO is discussed as a nonredox catalyst for hydrocarbon conversion reactions [17–22]. Li^+O^- sites are proposed to abstract atomic hydrogen from the hydrocarbon-generating radicals, which then desorb to start a chain propagation reaction in the gas phase. The catalytic activity of the solid exhibits a strong correlation to the amount of removable oxygen that is apparently destabilized by Li^+ ions [21,23].

Along with the generation of $[Li^+O^-]$ centers, an alternative mechanism that involves surface F-centers as active sites has been put forward [24,25]. A direct theoretical comparison of the associated energetics was made recently using electronic structure techniques based on DFT calculations. This provided

* Corresponding author. Fax: +43 1 25077 3890.
E-mail address: odiwald@mail.zserv.tuwien.ac.at (O. Diwald).
[1] Present address: Department of Chemical Physics, Fritz-Haber-Institute of the Max-Planck-Society, Faradayweg 4-6, D-14195 Berlin, Germany.

0021-9517/$ – see front matter
doi:10.1016/j.jcat.2007.01.008

relevant clues that binding of a hydrogen atom (originating from, e.g., hydrogen abstraction from CH_4) to an O^- ion is energetically more favorable than binding to an F-center [26].

Thermal treatment affects the material properties of Li-doped MgO polycrystals in the following ways:

(i) At elevated temperatures, the loss of structural oxygen of Li-doped MgO is facilitated. The concomitant increase in the oxygen vacancy concentration gives rise to p-type conductivity [27,28], which is enhanced compared with pure MgO above 873 K and prevails as a conduction mechanism at 1170 K. The electronic properties of a solid are related to the catalytic performance of doped oxide materials, because molecule activation generally occurs via charge transfer between the catalyst surface and the adsorbate.

(ii) Li^+ ions affect particle morphology. The dominant mechanism of Li incorporation involves the generation of hole centers, which—after segregation into the surface—destabilize low-index planes at higher coverages. Octahedrally shaped MgO-based crystals expressed by (111) planes are expected on the basis of theoretical investigations [29]. In fact, Hargreaves et al. [30] reported that Li-induced sintering of the crystallites is accompanied by loss of the regular morphology of the MgO precursor.

(iii) The thermal stability of the doped polycrystals is significantly decreased compared with undoped MgO. This presents a practical limitation, because the increase in grain size is equivalent to the decrease in chemically active surface area. XRD measurements have revealed the absence of any phase impurity, such as Li_2O, Li_2CO_3, or LiOH in Li^+-doped MgO particles, containing <10 at% Li^+ [16].

The description of reactive surface sites by spectroscopy at room temperature and below represents a useful approach for the characterization of relevant adsorption sites on the catalyst surface [31], although the corresponding experiments must be carried out under conditions much different than those during a catalytic reaction cycle.

Doping polycrystalline materials with impurities—which has a profound effect on the surface reactivity of the host oxide but do not alter the bulk structure—can represent an approach to quantifying the number of reactive sites on pure MgO particles. We produced Li^+-doped MgO nanoparticles using the chemical vapor deposition (CVD) technique and characterized Li^+ ion-induced changes on the surface of the resulting nanoparticles. IR spectroscopy and electron paramagnetic resonance (EPR) identified three characteristic types of surface defects: sites that dissociatively activate molecular hydrogen [32–34], oxygen-anion deficient arrays acting as electron traps [35–37], and surface cations complexing superoxy species O_2^- [38,39].

On the basis of Li^+-induced surface changes related to the total Li^+ content, an estimate for the number of chemically relevant surface sites on doped and undoped nanoparticles is given.

2. Experimental

MgO and Li-doped MgO nanoparticles were prepared by CVD based on the reaction of metal vapor (Mg: Johnson Matthey, 99.98%; Li: Aldrich, 99.9%) with O_2 (Messer Griessheim, 99.998%). The flow reactor system comprises a quartz glass tube and an inner stainless steel tube mounted concentrically inside a cylindrical furnace. Ar gas flows through the inner stainless steel tube and transports the metal atoms (magnesium vaporized at 900 K and lithium vaporized at 760–860 K, depending on the Li content required [40]) to a combustion zone, in which the reaction with oxygen coming from the outer quartz glass tube leads to the formation of nanometer-sized oxide particles. These are then deposited at the downstream end within a stainless steel net. Mg and Li concentrations were determined by atomic absorption spectroscopy (Perkin Elmer 2280) using hollow cathode lamps. The relative concentration of Li and Mg was constant over a production period of 30 min. Composition analysis of samples before and after annealing under high-vacuum conditions revealed that about 50% of the original Li content was lost during activation via evaporation. The samples were also checked for Fe contamination, which can originate from the stainless steel tube of the CVD reactor system; Fe at concentrations above 10 ppm was excluded on the basis of AAS measurements. For specific surface area determination, BET adsorption isotherms were measured by N_2 physisorption at 77 K.

The IR experiments were performed in an appropriate sample cell that allows sample activation at high-vacuum conditions with a base pressure above 5×10^{-6} mbar. Samples, in the form of hand-pressed, self-supporting wafers, were measured in the IR transmission mode with a Bruker IFS 113v spectrometer. A total of 300 scans were accumulated for one spectrum to obtain a reasonable signal-to-noise ratio. The spectral resolution was 3 cm^{-1}. For IR and EPR spectroscopic measurements, the respective material was subjected to thermal treatment up to 1173 K. First, the sample was heated at a rate of 5 K min^{-1} to 873 K and exposed to oxygen at this temperature to remove organic contaminants. Finally, the sample was heated to 1173 K at $p < 5 \times 10^{-6}$ mbar and kept under these conditions for 1–2 h to dehydroxylate the particle surfaces. Occasional impurities, such as carbonaceous species, were completely eliminated by this procedure. In contrast to pure MgO, Li-doped samples showed absorptions of minor intensity in the OH region with band positions different than those observed on pure MgO after chemisorption of H_2. The spectra shown in Fig. 2 were obtained by subtracting spectra measured in the presence of 100 mbar from those acquired directly after thermal activation and cooling to room temperature.

For EPR measurements, the respective powder sample was filled into an EPR tube, which was then attached to a high-vacuum pumping stage, providing a base pressure $p < 5 \times 10^{-6}$ mbar. The same activation procedure as in the IR study was applied. UV exposure for the generation of paramagnetic surface defects was carried out using a 300-W xenon lamp (Oriel) equipped with a water filter. X-band EPR measurements were performed with a Bruker EMX 10/12 spectrometer us-

ing an ER 4102 ST standard rectangular resonant cavity in the TE_{102} mode. Low-temperature measurements were done with a Dewar filled with liquid nitrogen ($T = 77$ K). Ten accumulated scans provided a reasonable signal-to-noise ratio. The g values were determined on the basis of a DPPH standard (Aldrich 25,762-1).

3. Results

3.1. Thermal stability

Fig. 1 plots the specific surface area values of pure and Li^+-doped MgO nanoparticles as a function of thermal activation at temperatures between 473 and 1173 K. For pure MgO, 470 $m^2\,g^{-1}$ was measured immediately after the CVD process (Fig. 1a). On thermal activation, the specific surface area was maintained up to 673 K. Between 673 K and 873 K, however, the surface area decreased to 300 $m^2\,g^{-1}$ and remained constant thereafter at least up to 1173 K. After thermal activation, the pure MgO nanocrystals had a particle size of 7 nm. For the Li^+-doped samples, the specific surface area was critically dependent on the Li^+ concentration and decreased with increasing amounts of Li^+ (Figs. 1b–1d). All of these curves had a decay at 673–873 K in common.

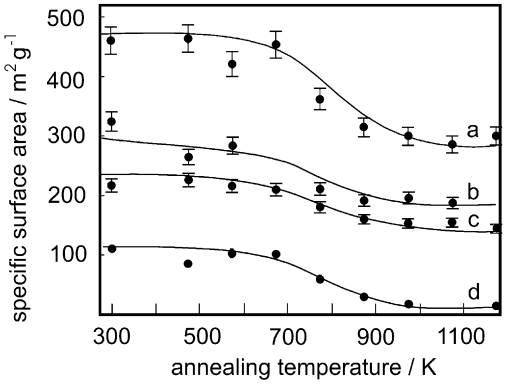

Fig. 1. Dependence of the specific surface area on the Li concentration and thermal treatment of Li-doped MgO nanoparticles: (a) pure MgO, (b) 0.02 at% Li, (c) 0.1 at% Li, (d) 2.0 at% Li.

3.2. IR spectroscopy: surface hydroxyl and hydride groups

The IR spectra in Fig. 2 demonstrate hydrogen chemisorption in the presence of 100 mbar H_2 on undoped and doped MgO nanoparticles that had been dehydroxylated at 1173 K. For undoped MgO nanoparticles, it is generally accepted that at room temperature, hydrogen splitting proceeds via two different heterolytic pathways according to [32,33,36]

$$Mg^{2+}\text{–}O^{2-} + H_2 \rightarrow Mg^{2+}H^-\text{–}O^{2-}H^+. \quad (1)$$

The corresponding IR spectrum (Fig. 2, bottom) clearly reveals two pairs of OH and MgH stretching bands, which are associated with irreversible (3712 and 1130 cm^{-1}) and a reversible H_2-splitting processes (3462 and 1325 cm^{-1}) [32,33]. Profound spectral changes occurred with increasing Li^+ concentration (Fig. 2). The OH and MgH stretching bands specific to pure MgO lost intensity, and new bands grew in the OH and MeH stretching region. At a concentration of 0.2 at% (Fig. 3, top) the MgO-specific OH and MgH bands were lost. Obviously, a Li concentration of 0.2 at% Li (bulk plus surface) effectively replaced all MgO-specific IR bands after thermally induced Li^+ segregation.

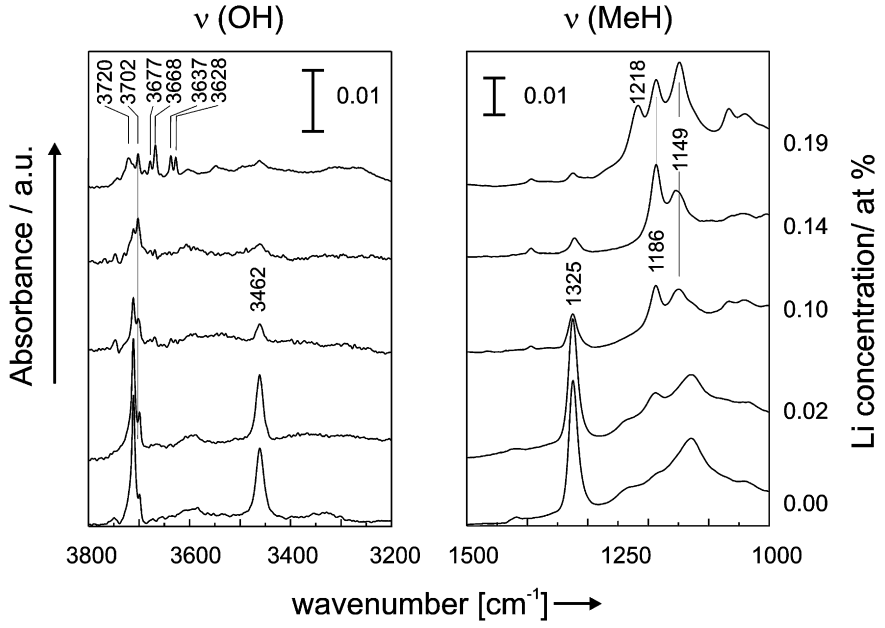

Fig. 2. Room temperature IR spectra of chemisorbed hydrogen species obtained on Li^+-doped MgO nanoparticles. The patterns shown were obtained by subtracting the sample spectra before admission of 100 mbar H_2 from those recorded thereafter. The spectra of Li-doped samples were not normalized with respect to comparable surface areas.

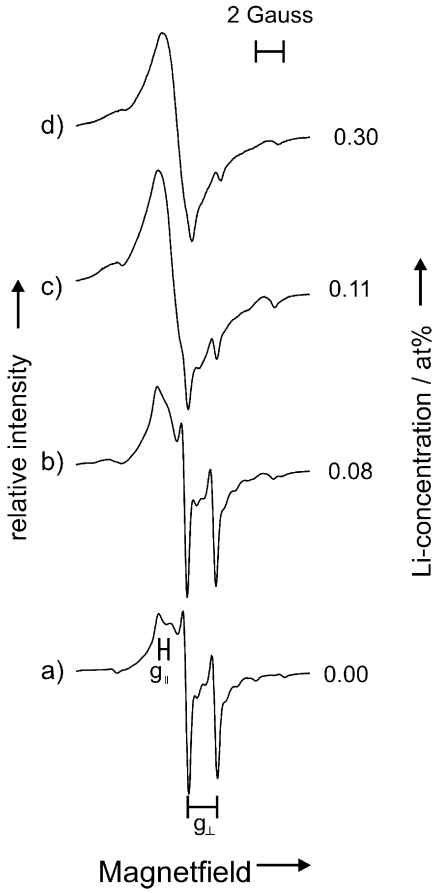

Fig. 3. Electron paramagnetic resonance spectra of trapped electron centers on pure (a) and Li-doped MgO nanoparticles (b–d). The paramagnetic centers were generated by UV exposure in the presence of 10 mbar H_2 at room temperature.

3.3. EPR spectroscopy: surface-trapped electrons

After thermal activation at 1170 K and cooling, Li^+-doped MgO nanoparticles showed no paramagnetic center at 77 K. To generate trapped electron centers as paramagnetic surface probes, samples of various Li^+ contents were exposed to hydrogen and UV light. On pure high-surface area MgO, such a treatment led to the production of $(H^+)(e^-)$ centers that are intensively investigated surface probes [37,41,42]. The characteristic EPR signature revealed significant electron spin interaction with the proton of an adjacent OH group appearing as a superhyperfine splitting of the resonance lines into a doublet [41,43]. Fig. 3a shows a typical color center signal measured on MgO nanocubes [35,44]. The admixture of Li^+ doping gradually replaced the characteristic signature with a broad isotropic signal (Figs. 3b–3b) that does not change its contour within the microwave power range of 10^{-6}–10^{-3} W. At a Li^+ concentration of 0.3 at%, the MgO-specific color center signature was essentially lost.

3.4. EPR spectroscopy: adsorbed O_2^- ions stabilized by surface cations

Admission of molecular oxygen to MgO surfaces with trapped electrons destroys the corresponding signals in Fig. 2

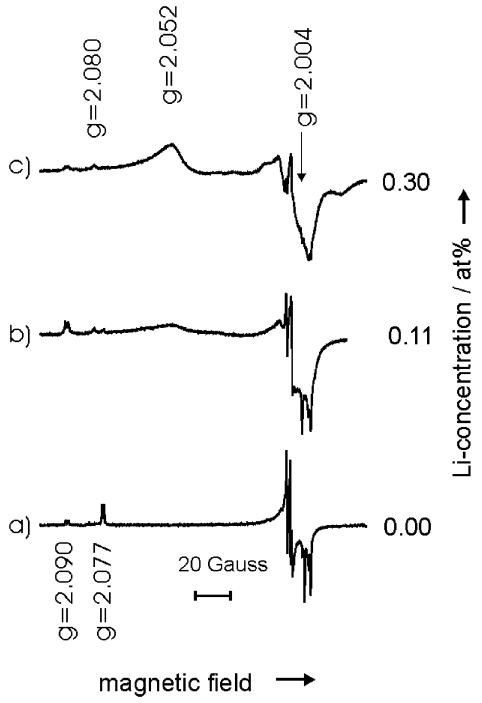

Fig. 4. Electron paramagnetic resonance spectra of superoxide anions O_2^- on pure and Li^+-doped MgO nanoparticles. The surface radicals were generated by addition of molecular oxygen to oxide nanoparticles which contain surface trapped electrons (Fig. 3) and evacuation thereafter. Acquisition temperature was 77 K.

and gives rise to the formation of adsorbed superoxy species O_2^- according to

$$\left(Mg^{2+}\right)_n e^- + O_2 \rightarrow \left(Mg^{2+}\right)_n O_2^-. \quad (2)$$

This also applies for Li^+-doped MgO nanoparticles, as demonstrated by the EPR spectra in Fig. 4, in which orthorhombic signal patterns of the radical anions are clearly observable. The g_{xx} and g_{yy} signals overlap, but the well-separated g_{zz} components, which are subject to the local crystal field gradient at the adsorption site, present a site-sensitive probe for surface cations [38]. On undoped MgO, essentially two O_2^- species complexed by differently coordinated surface Mg^{2+} cations can be identified from the EPR spectrum in Fig. 4a. All components of the g tensor, including g_{zz} at 2.077 and at 2.090, exhibit a distinct hyperfine interaction with the proton of a nearby hydroxyl group (^1H shf splitting), consistent with previous observations given in Table 1 [45,46]. A third O_2^- type characterized with $g_{zz} = 2.080$ can be found on samples with 0.11 and 0.30 at% Li^+ (Fig. 4). The g-matrix of this signal lacks ^1H shf splitting effects and indicates the absence of a significant interaction between the adsorbed oxygen radical and a hydroxyl group in close vicinity. The fact that such species have also been observed in previous experiments on pure MgO [46] suggests that it is not directly associated with Li^+ cations as coordinating surface sites. With increasing Li^+ content, all MgO-specific O_2^- sites lost relative intensity (Figs. 4b–4c), and above 0.2 at% Li^+ the most intense MgO component at $g_{zz} = 2.077$ is absent. Furthermore, the ^1H shf splitting effect cannot be resolved at higher Li^+ concentrations.

Table 1
Paramagnetic oxygen species observed on pure and Li-doped MgO nanocrystals. The accuracy for g factor determination is $\pm 10^{-4}$

O_2^- species						References
g_{xx}	g_{yy}	g_{zz}	a_{xx} [G]	a_{yy} [G]	a_{zz} [G]	
A						
2.0019	2.0085	2.0902	5.10	2.97	1.40	[53,54,56]
B						
2.0017	2.0086	2.0769	3.76	2.06	1.10	[53,54,56]
B′						
2.0017	2.0086	2.0802	–	–	–	[46,56]
$[Li^+O^-]$ species						
	$g_\perp = 2.052$			$g_\parallel = 2.004$		[47,48]

A broad and intense feature at $g = 2.052$ appears (Fig. 4c). Comparison with literature values reveals that the g parameters $g_\perp = 2.054$ and $g_\parallel = 2.004$ (Table 1) are consistent with O^- hole centers in conjunction with adjacent Li^+ ions [47,48] rather than with the EPR signature of O_2^- ions [38,39]. As reported by Lunsford et al. [48], on powders, such centers are generated at temperatures above 673 K and stabilized thereafter if quenching in liquid O_2 to 77 K is applied. In the present study, adding H_2 to a sample (characterized by the top spectrum in Fig. 4) led to only a partial signal reduction ($\Delta < 10\%$) of the feature at $g = 2.054$ and thus indicates reduced chemical reactivity compared with hole centers present on pure MgO nanocubes [44].

4. Discussion

Traces of Li ions significantly affected the thermal stability of the MgO-based materials. Already during particle generation in the combustion flame inside the CVD reactor, significant grain coarsening occurred, as derived from the initial values of the BET measurements (Fig. 1). After subsequent thermal activation under high-vacuum conditions, a Li^+ concentration decrease of about 50% was observed. This is in line with other reports of Li_2O evaporation during sintering of Li^+-doped MgO materials [49]. By favoring the formation of anion vacancies, Li^+ ions enhance ion mobility at elevated temperatures [27,28] and segregate from the bulk into the nanoparticle surface. In fact, quantum chemical calculations have suggested that Li^+ cations embedded in the MgO nanoparticles segregate during an appropriate annealing procedure into the surface, where they preferentially substitute the lowest-coordinated Mg^{2+} cations to compensate for local deviations from stoichiometry [50,51].

The IR and EPR spectroscopic data obtained for Li^+-doped MgO nanoparticles (Figs. 2 and 4) have one feature in common: After thermal treatment, Li^+ ions localize either in the near-surface region or in the surface of the MgO-based material, where they significantly alter surface reactivity. Irrespective of the specific surface reaction, hydrogen activation (Fig. 2), electron trapping (Fig. 3), or electron transfer to molecular oxygen (Fig. 4), Li^+ admixture with a concentration of ca. 0.2 at% replaces all MgO-specific signals by qualitatively new spectroscopic features. It was shown that undoped high-surface area MgO materials (compare, e.g., CVD MgO nanocubes [18,33,35] with MgO obtained via the controlled thermal decomposition of hydroxides [5,32,37]) have different particle morphologies but show identical spectroscopic fingerprints in terms of IR band positions [32,33] and g factors [35,37]. This rules out the possibility that MgO particle morphology variations give rise to different spectroscopic features and furthermore proves that the spectroscopic effects observed for Li-containing samples are directly related to the presence of Li ions.

Obviously there is no preferential depletion of either electron-trapping sites or sites active in hydrogen splitting with increased Li^+ concentration. This may be explained in two different ways: either Li^+ influences the respective underlying sites accidentally to the same extent, or the sites involved in hydrogen chemisorption and electron-trapping are identical. The substitution of Mg^{2+} cations by Li^+ ions can also lead to long-range effects regarding the reactivity of local MgO-based surface structures, such as inverse steps proposed for H_2 splitting [32] or edges as electron-trapping sites [37].

Surface-trapped electrons react instantaneously with O_2. It was shown by OH probe spectroscopy that O_2^- sites characterized by a g_{zz} component at 2.077 are directly associated with the trapping site that previously hosted the $(H^+)(e^-)$ center [33,34,45]. Structural elements, such as edges and step edges made of four-coordinated cations and anions, can be active for electron trapping and the complexation of O_2^- ions, as demonstrated by the good agreement between experimental and theoretical data [36,37,52,53]. The relative contribution of the O_2^- at $g_{zz} = 2.077$ decreased with increasing Li^+ content compared with the less strongly bound O_2^- with g_{zz} at 2.090. This again is in line with quantum mechanical calculations predicting that the lowest-coordinated Mg^{2+} cations are replaced by thermally induced Li^+ segregation [50]. Regarding the O_2^-, which is associated with a significantly smaller local crystal field splitting with $g_{zz} = 2.090$, there is agreement that the complexing cation must be fivefold located in a (100) microplane [54,55]. The electronic interaction between the O_2^- ion and a nearby OH group would explain the stability of this adsorption complex [56].

As a surprising result, an EPR signal at $g = 2.052$ emerged after color centers were bleached on thermally stable MgO nanoparticles at Li^+ concentrations >0.2 at% (Fig. 4d). This feature was observed on pure Li_2O powders and assigned to a stable surface O^- species. It is likely to be present on Li^+-doped MgO nanoparticles. Owing to the comparatively large half width of this signal component, it is detectable only at higher concentrations. With the less tightly bound electrons of the oxygen anions surrounding the low-coordinated Li^+, the electron affinity of the O_2 molecules might facilitate electron transfer from O^{2-} to O_2.

The surface concentration of defects on pure MgO nanoparticles can be estimated by evaluating the Li^+ concentration effect on the MgO-specific reactivity pattern. The following assumptions can be made:

(i) The total amount of Li^+ segregates into the subsurface or surface region. Correspondingly, the estimated concentra-

tion presents an upper limit, because Li^+ ions that remain dissolved in the bulk cannot be excluded.

(ii) The particle surface is assumed to be smooth in the sense that the specific surface area can be directly related to the particle size on the basis of particle shape. This assumption is valid for pure MgO nanocubes in which the average edge length of the cube is consistent with the measured values for the specific surface area [1].

With respect to various methods of determining average particles size, D (i.e., TEM, X-ray diffraction, and BET), the use of BET specific surface areas (S_{BET})—where the cross-sectional area of N_2 (in $nm^2\,molecule^{-1}$) serves as principle input parameter—provides the most straightforward approach. The respective formula $S_{BET} = 6(1/\rho \cdot D_{BET})$, with ρ as the density of the solid, applies for cubes as well as for spheres and thus for all conceivable MgO particle morphologies. In case of rougher particle surfaces, the derived value for D may deviate from the true value but will not affect the final result, that is, the maximum concentration of reactive surface sites.

A specific surface area of 110 $m^2\,g^{-1}$ for MgO particles doped with 0.2 at% Li (Fig. 1) corresponds to an average edge length of 15.2 nm for cubical-shaped particles. Such a particle contains 3.8×10^5 ions in total and 760 Li^+ ions if doped with 0.2 at% Li^+. With a total number of 1.5×10^4 surface cations and perfect Li^+ segregation into the surface [assumption (i)], 4.8% of all surface cations would be Li^+. This number also applies for spherical particles with a diameter of 15.1 nm [57]. If we exclude long-range effects, where a Li^+ ion affects the reactivity of more than one coordination sphere, this suggests that <3% of all cationic surface sites are involved in surface processes, such as hydrogen chemisorption and electron-trapping. This estimate corresponds to an upper limit, because complete segregation of Li^+ from the bulk into the surface and atomically plane surfaces were adopted in the model applied. The underestimation of smaller particle sizes (an inherent shortcoming of the BET approach) implies that the actual surface site concentration is again <3%. It is interesting to note that on an ideal MgO cube of 15.2 nm edge length, this value corresponds to the fraction of surface cations located on the edges.

5. Conclusion

Admixtures of small amounts of Li to Mg vapor during the chemical vapor deposition process decrease the stability of the resulting oxide nanoparticles. After thermally induced surface segregation, Li^+ ions effectively alter all MgO-specific spectroscopic fingerprints, such as IR active hydroxyls and hydrides, surface-trapped electrons, and adsorbed oxygen radicals. We conclude that Li^+ ions preferentially move into surface sites associated with low-coordinated ions and enhanced surface reactivity. Doping of oxide nanostructures with chemically active impurities provides an efficient way to estimate the concentration of reactive surface defects on the undoped material.

Acknowledgments

Support was provided by the Austrian Fonds zur Förderung der wissenschaftlichen Forschung (FWF Grants P14731-CHE and P17770-N11). The authors thank Dr. Andreas Limbeck and Dr. Markus Handler (Institute of Chemical Technologies and Analytics, Vienna University of Technology) for an independent quantitative analysis of the Li concentration in MgO nanoparticles using ICP-AES.

References

[1] S. Stankic, M. Müller, M. Sterrer, J. Bernardi, O. Diwald, E. Knözinger, Angew. Chem. Int. Ed. 44 (2005) 4917.
[2] V.E. Henrich, P.A. Cox, The Surface Science of Metal Oxides, Cambridge Univ. Press, 1996.
[3] C. Barth, C.R. Henry, Phys. Rev. Lett. 91 (2003) 196102.
[4] M. Sterrer, E. Fischbach, T. Risse, H.-J. Freund, Phys. Rev. Lett. 94 (2005) 186101.
[5] G. Spoto, E.N. Gribov, G. Ricchiardi, A. Damin, D. Scarano, S. Bordiga, C. Lamberti, A. Zecchina, Prog. Surf. Sci. 76 (2004) 71.
[6] R. Richards, W.F. Li, S. Decker, C. Davidson, O. Koper, V. Zaikovski, V. Volodin, T. Rieker, K.J. Klabunde, J. Am. Chem. Soc. 122 (2000) 4921.
[7] Z. Dohnalek, G.A. Kimmel, D.E. McCready, J.S. Young, A. Dohnalkova, R.S. Smith, B.D. Kay, J. Phys. Chem. B 106 (2002) 3526.
[8] S. Stankic, J. Bernardi, O. Diwald, E. Knözinger, J. Phys. Chem. B 110 (2006) 13866.
[9] A. Corma, S. Iborra, Adv. Catal. 49 (2006) 239.
[10] M.L. Bailly, C. Chizallet, G. Costentin, J.M. Krafft, H. Lauron-Pernot, M. Che, J. Catal. 235 (2005) 413.
[11] I.M. Mellor, A. Burrows, S. Coluccia, J.S.J. Hargreaves, R.W. Joyner, C.J. Kiely, G. Martra, M. Stockenhuber, W.M. Tang, J. Catal. 234 (2005) 14.
[12] J. Cunningham, C. Healy, D. McNamara, S. O'Brien, Catal. Today 2 (1988) 557.
[13] S. Coluccia, Stud. Surf. Sci. Catal. 21 (1985) 5.
[14] P. Hofmann, E. Knözinger, O. Diwald, A. Mustafa, Ber. Bunsen-Ges. Phys. Chem. 101 (1997) 1722.
[15] S. Stankic, M. Sterrer, P. Hofmann, J. Bernardi, O. Diwald, E. Knözinger, Nano Lett. 5 (2005) 1889.
[16] H. Aitani, H. Yamada, T. Nishio, T. Shiono, S. Imamura, M. Kudo, S. Hasegawa, T. Tanaka, S. Yoshida, J. Phys. Chem. B 104 (2000) 10133.
[17] L. Lefferts, K. Seshan, B. Mojet, J. van Ommen, Catal. Today 100 (2005) 63.
[18] T. Ito, J. Wang, C.H. Lin, J.H. Lunsford, J. Am. Chem. Soc. 107 (1985) 5062.
[19] J.H. Lunsford, Angew. Chem. Int. Ed. 34 (1995) 970.
[20] R. Orlando, F. Cora, R. Millini, G. Perego, R. Dovesi, J. Chem. Phys. 105 (1999) 351.
[21] L. Leveles, K. Seshan, J.A. Lercher, L. Lefferts, J. Catal. 218 (2003) 296.
[22] C.R.A. Catlow, S.A. French, A.A. Sokol, J.M. Thomas, Philos. Trans. R. Soc. A 363 (2005) 913.
[23] L. Leveles, K. Seshan, J.A. Lercher, L. Lefferts, J. Catal. 218 (2003) 307.
[24] M.-C. Wu, C.M. Truong, D.W. Goodman, Phys. Rev. B 46 (1992) 12688.
[25] M.-C. Wu, C.M. Truong, K. Coulter, D.W. Goodman, J. Catal. 140 (1993) 344.
[26] L.K. Dash, M.J. Gillan, Surf. Sci. 549 (2004) 217.
[27] I. Balint, K.I. Aika, Appl. Surf. Sci. 173 (2001) 296.
[28] M.M. Tardio, R. Ramirez, R. Gonzalez, Y. Chen, Phys. Rev. B 66 (2002) 134202.
[29] G.W. Watson, Radiat. Eff. Defects Solids 157 (2002) 773.
[30] J.S. Hargreaves, G.J. Hutchings, R.W. Joyner, C.J. Kiely, J. Catal. 135 (1992) 576.
[31] M. Sterrer, T. Berger, O. Diwald, A. Allouche, E. Knözinger, Top. Catal. (2006), in press.
[32] E.N. Gribov, S. Bertarione, D. Scarano, C. Lamberti, G. Spoto, A. Zecchina, J. Phys. Chem. B 104 (2004) 16174.

[33] O. Diwald, P. Hofmann, E. Knözinger, Phys. Chem. Chem. Phys. 1 (1999) 713.
[34] O. Diwald, M. Sterrer, E. Knözinger, Phys. Chem. Chem. Phys. 4 (2002) 2811.
[35] M. Sterrer, T. Berger, S. Stankic, O. Diwald, E. Knözinger, Chem. Phys. Chem. 5 (2004) 1695.
[36] D. Ricci, C. Di Valentin, G. Pacchioni, P.V. Sushko, A.L. Shluger, E. Giamello, J. Am. Chem. Soc. 125 (2003) 738.
[37] M. Chiesa, M.C. Paganini, G. Spoto, E. Giamello, C. Di Valentin, A.D. Vitto, G. Pacchioni, J. Phys. Chem. B 109 (2005) 7314.
[38] M. Che, A.J. Tench, Adv. Catal. 32 (1983) 1.
[39] M. Anpo, M. Che, B. Fubini, E. Garrone, E. Giamello, M.C. Paganini, Top. Catal. 8 (1999) 189.
[40] J. Schuh, Diploma thesis, Vienna University of Technology, 2001.
[41] E. Giamello, M.C. Paganini, D.M. Murphy, A.M. Ferrari, G. Pacchioni, J. Phys. Chem. B 101 (1997) 971.
[42] M. Sterrer, T. Berger, O. Diwald, E. Knözinger, P. Sushko, A. Shluger, J. Chem. Phys. 123 (2005) 0647141.
[43] A.J. Tench, R.L. Nelson, J. Colloid Interface Sci. 26 (1968) 364.
[44] O. Diwald, T. Berger, M. Sterrer, E. Knözinger, Stud. Surf. Sci. Catal. 140 (2001) 237.
[45] O. Diwald, G. Martra, E. Knözinger, J. Chem. Phys. 111 (1999) 6668.
[46] O. Diwald, Ph.D. thesis, Vienna University of Technology, 2000.
[47] M.M. Abraham, W.P. Unruh, Y. Chen, Phys. Rev. B 10 (1974) 3540.
[48] J.-X. Wang, J.H. Lunsford, J. Phys. Chem. 90 (1986) 5883.
[49] T. Norby, A. Anderson, Appl. Catal. 71 (1991) 89.
[50] M. Nolan, G.W. Watson, Surf. Sci. 586 (2005) 25.
[51] D.W. Lewis, R.W. Grimes, C.R.A. Catlow, J. Mol. Catal. A 100 (1995) 103.
[52] D. Ricci, G. Pacchioni, P.V. Sushko, A.L. Shluger, Surf. Sci. 542 (2003) 293.
[53] M. Chiesa, E. Giamello, M.C. Paganini, Z. Sojka, D.M. Murphy, J. Chem. Phys. 116 (2002) 4266.
[54] E. Giamello, D. Murphy, E. Garrone, A. Zecchina, Spectrochim. Acta A 49 (1993) 1323.
[55] E. Giamello, E. Garrone, P. Ugliengo, M. Che, A.J. Tench, J. Chem. Soc. Faraday Trans. I 85 (1989) 1373.
[56] O. Diwald, E. Knözinger, J. Phys. Chem. B 106 (2002) 3495.
[57] With a specific surface area of 110 $m^2\ g^{-1}$ the diameter of ideal monodisperse nanospheres corresponds to 15.2 nm with 2×10^5 ions per particle and 8300 surface Mg^{2+} ions.